Modeling of Multi-Layer Anti-Reflective Structuring in a Silicon Lens

by

Spencer C. Brugger

A thesis submitted to the faculty of the
University of Colorado in partial fulfillment
of the requirements for the award of
departmental honors in the department of Engineering Physics
in the College of Engineering and Applied Sciences
October 29, 2012

Committee Members:

Prof. Jason Glenn (Thesis Advisor, Physics)

Prof. Jeremy Darling (APS)

Prof. John Cumalat (Physics)

This thesis entitled:
Modeling of Multi-Layer Anti-Reflective Structuring in a Silicon Lens
written by Spencer C. Brugger
has been approved for the College of Engineering and Applied Sciences Engineering Physics

Jason Glenn

Prof. Jeremy Darling

Prof. John Cumalat

Date

The final copy of this thesis has been examined by the signatories, and we find that both the content and the form meet acceptable presentation standards of scholarly work in the above mentioned discipline.

Brugger, Spencer C. (B.S. Engineering Physics)

Modeling of Multi-Layer Anti-Reflective Structuring in a Silicon Lens

Thesis directed by Prof. Jason Glenn

Anti-reflection coatings are typically applied to a surface to reduce optical reflection at an interface. These coatings are usually in the form of thin films with matching refractive indices, but only are efficient for a small waveband. This idea can be mimicked by structuring (e.g. cutting parallel grooves) on a surface to change the effective dielectric constant and can potentially be efficient across a larger band of wavelengths. Surface structuring methods for anti-reflection purposes has been shown to be a viable method at the National Institute of Standards and Technology (NIST) and at the University of Michigan [1].

Two cameras are being developed for CCAT: The Short-Wavelength Camera (SWCam) and the Long-Wavelength Camera (LWCam). SWCam will have a primary band centered at 350μm and LWCam will cover 6 spectral bands from 750μm to 3.3mm. SWCam may also cover secondary bands at 450 and 200μm as well. These bands are too wide for thin film anti-reflective coatings to be efficient and materials with the appropiate index of refraction do not exist.

Silicon is chosen as the lens material due to its low loss in the submillimeter band. The downside to silicon is a high index of refraction which causes an increase in reflection at the air-silicon interface and so a broadband anti-reflection solution must be achieved.

I have modeled the physical situation and have used the model to do simulations to verify the performance of anti-reflective structuring. The model allows for multiple layers of structures having different depths and widths. We are able to specify wavelength and angle of incidence, allowing one to integrate over full Gaussian beams. We have confidence in the model due to it producing known solutions in limiting cases. Future work entails further simulations to determine what tolerances we must achieve in fabricating the lenses to allow for reflections of less than 1% across the full bandwidth.

Contents

Chapter

Chapter 1

Introduction

1.1 CCAT

CCAT is being designed to be located at 5600m on Cerro Chajnantor in the Andes mountains in Chile. The goal of CCAT is to have the capability for deep, large area multicolor submillimeter surveys. Science objectives include galaxy formation and evolution throughout the history of the Universe; hot gas pervading clusters of galaxies; star formation, protoplanetary disks, and debris disks in the Milky Way galaxy; and Kuiper belt objects in the outer reaches of the Solar System. The telescope will have a 25m diameter aperture with a 1 degree field of view and 3.5 arcseconds of angular resolution at 350μm. The telescope aims to function at wavelengths of 200 - 2,200μm [2]. To accomplish this, two cameras are being developed for CCAT: the Long-Wavelength Camera (LWCam) and the Short-Wavelength Camera (SWCam).

1.2 LWCam

LWCam will have a 20 arcminutes field-of-view and will cover 6 spectral bands from 750μm to 3.3mm. The camera will utilize either microwave kinetic inductance detectors (MKIDs) or transition-edge sensor (TESs), with MKIDs being the most attractive option due to the ease of multiplexing. TESs have recently been successful (ACT, BICEP2, Keck Array and others) so they are being considered. Because of LWCam's angular resolution, wide field-of-view, broad spectral coverage, and large mapping speed, the camera will be useful in studies of dusty, star-forming galaxies [3].

1.3 SWCam

SWCam will also use MKID technology, but will have the primary band centered at 350μm. The goal of SWCam is also to observe dusty, star-forming galaxies, but will observe at shorter wavelengths than LWCam [4]. The combination of LWCam and SWCam will allow for CCAT to study a large continuum in spectra.

Chapter 2

Two Layer Dielectric

2.1 Two Layer Case

Imagine we have the optical system of Air - Layer1 - Layer2 - Air. Layer1 has index of refraction n_1 and thickness d_1. Similarly for Layer2. We have 3 interfaces (Air/Layer1, Layer1/Layer2, and Layer2/Air) that we can assign reflection and transmissions coefficients to (I will call them r_i and t_i, where i is the 1st, 2nd, or 3rd interface). A schematic of this system can be seen in figure[2.1].

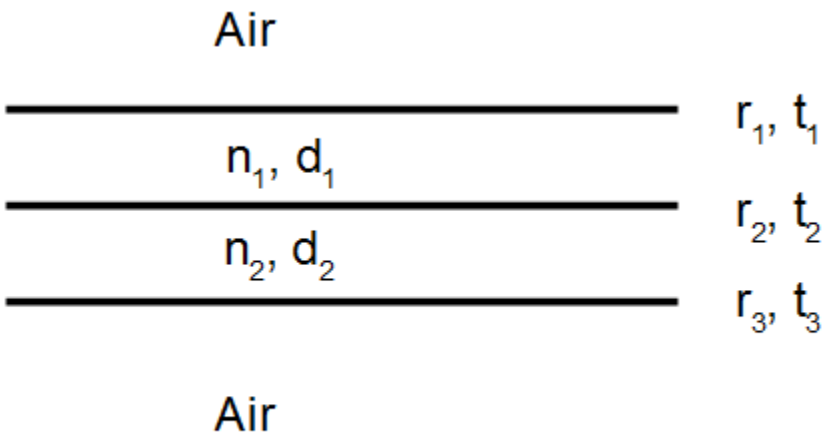

Figure 2.1: Schematic of two layer case

2.2 Calculating the Transmitted Field

The reflection coefficients are calculated from the Fresnel equations as $r = \frac{n_2 \cos\theta_t - n_1 \cos\theta_i}{n_2 \cos\theta_t + n_1 \cos\theta_i}$ [5] for a wave traveling in a medium of n_1 towards a medium of n_2. Assuming no absorption, $R + T = r^2 + \frac{n_t \cos\theta_t}{n_i \cos\theta_i} t^2 = 1$ so the transmission coefficient is just $t = \sqrt{\frac{n_i \cos\theta_i}{n_t \cos\theta_t}(1 - r^2)}$.

The delay in phase, δ, of two adjacent rays (one of which has been reflected) is given as $\delta = k_0 \Lambda$, where $\Lambda = 2nd/\cos\theta_t$ and $k_0 = 2\pi/\lambda$ [5]. We can then find θ_t via Snell's Law. We then find δ_i for Layer1 and Layer2.

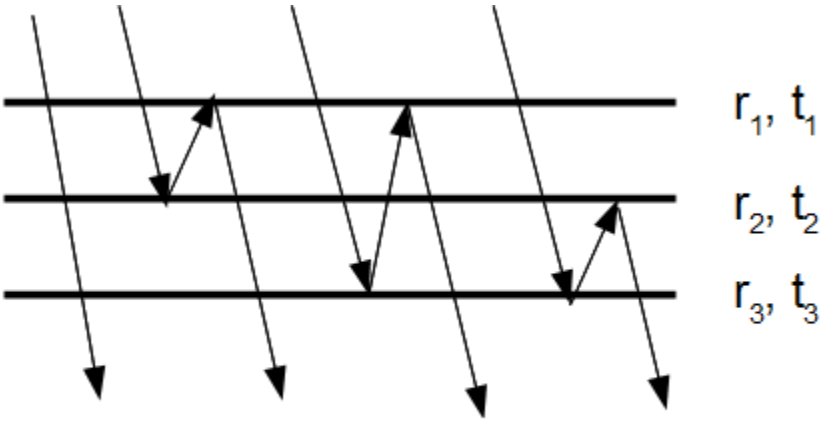

Figure 2.2: Schematic of a few cases of reflection for a two layer system

Now let us consider only the light that is transmitted through the entire system. Let E be the transmitted wave normalized to the original wave. If no reflections occur we will just have $E = t_1 t_2 t_3$ (this is the first wave drawn in figure[2.2]). Now let's consider a wave reflected on the second interface, which is then reflected off the first interface, and then transmitted out through the system (the second wave drawn in figure[2.2]). This would be written as $E = t_1 t_2 t_3 r_1 r_2 exp(-i\delta_1)$ with respect to the first wave. Similarly, if the bounce occurred between interface 3 and 2 (the fourth wave drawn in figure[2.2]), $E = t_1 t_2 t_3 r_2 r_3 exp(-i\delta_2)$. Another situation can occur: a wave is reflected between interface 3 and interface 1 and is transmitted between interface 2 twice (once

for each reflection) before leaving the system (the third wave drawn in figure[2.2]). This looks like $E = t_1t_2t_3r_3t_2r_1t_2exp(-i(\delta_1 + \delta_2))$. Additionally, we can observe any combination of these few cases.

For a transmitted wave we will always have the combination of $t_1t_2t_3$ effecting the amplitude and some combination of reflections. I claim that we can write any combination of reflections resulting in transmission as

$$E = t_1t_2t_3(r_1r_2e^{-i\delta_1})^m(r_2r_3e^{-i\delta_2})^n(r_1r_3t_2^2e^{-i(\delta_1+\delta_2)})^p$$

where m, n, and $p = 0, 1, 2, 3....$ It should be noted that there is an additional phase change of π for a reflected wave if the wave if traveling in a medium of n_1 and is reflected off a medium of n_2, where $n_2 > n_1$.

The amplitude of a transmitted wave reduces very quickly with the number of reflections so we can just do three nested for loops and computing will still go fairly quickly.

At the end we just sum up all the transmitted waves and find the transmitted irradiance by multiplying the total transmitted field by its complex conjugate:

$$E_{tot} = \sum E$$

$$I_t = E_{tot} * conj(E_{tot})$$

Now, although this does converge rather quickly, it is still not ideal to compute the transmitted field this way. Three nested for loops is fairly fast to compute, but when we get to the 5 layer case we would need 15 nested for loops which is not ideal. Since we end up summing all the transmitted waves, we can write the calculation as

$$E_{tot} = \sum_{m=0}^{m'}\sum_{n=0}^{n'}\sum_{p=0}^{p'} t_1t_2t_3(r_1r_2e^{-i\delta_1})^m(r_2r_3e^{-i\delta_2})^n(r_1r_3t_2^2e^{-i(\delta_1+\delta_2)})^p$$

Let m', n', and $p' \to \infty$, then we have the triple infinite sum:

$$E_{tot} = t_1 t_2 t_3 \sum_{m=0}^{\infty}\sum_{n=0}^{\infty}\sum_{p=0}^{\infty}(r_1 r_2 e^{-i\delta_1})^m (r_2 r_3 e^{-i\delta_2})^n (r_1 r_3 t_2^2 e^{-i(\delta_1+\delta_2)})^p$$

The infinite sum $\sum_{k=0}^{\infty}(\rho e^{-i\theta})^k$ will converge to $e^{-i\theta}/(e^{-i\theta}-\rho)$ given that $|\rho| < 1$. For any interface $r_i \leq 1$, and if $r_i = 1$ then the corresponding $t_i = 0$, so we can still apply the convergence of the above infinite sum to our calculation. This results in:

$$E_{tot} = \frac{t_1 t_2 t_3 e^{-2i(\delta_1+\delta_2)}}{(e^{-i\delta_1} - r_1 r_2)(e^{-i(\delta_1+\delta_2)} - r_1 r_3)(e^{-i\delta_2} - r_2 r_3)}.$$

This convenience allows us to compute the irradiance much quicker.

2.3 Sanity Checks

In the limit that Layer1 and Layer2 have the same index of refraction, we know that the fractional reflection should be zero when $\delta = 2m\pi, m = 1, 2, 3, ...$

For the case with $n_1 = n_2 = 2.5, d_1 = d_2 = 1$mm and normal incidence, the fractional reflection should be zero at wavelengths of $\lambda = 10/m$ millimeters, which is what we see in figure[2.3].

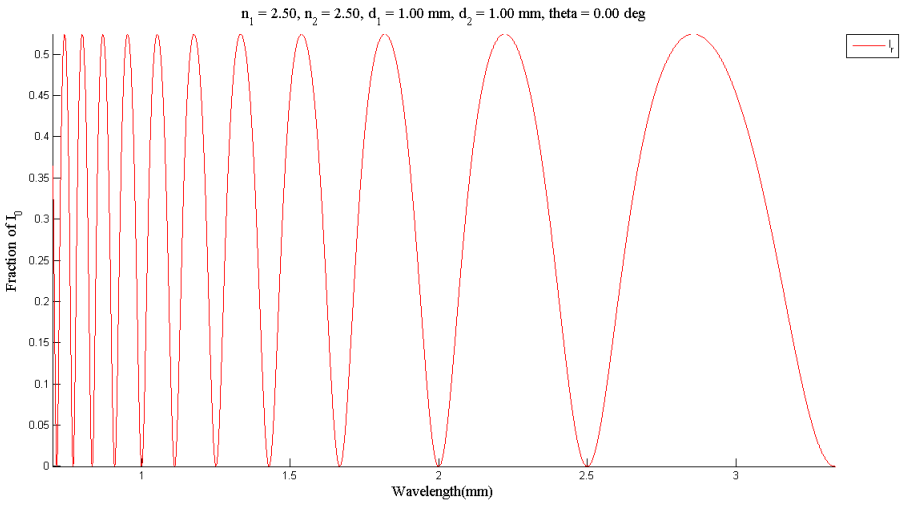

Figure 2.3: Two layer case where both layers have the same dielectric constant. We expect to see a minimum in fractional reflection at $\lambda = 10/m$ millimeters, $m = 1, 2, 3, ...$

We should also see a minimum at $\lambda = 5/m$ millimeters if the first layer is air, as in figure[2.4].

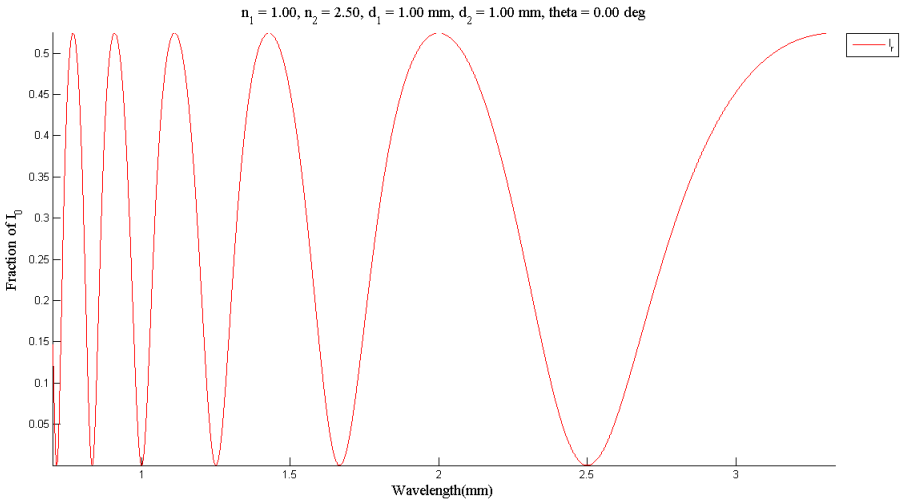

Figure 2.4: Two layer case where the first layer is air and the second layer has an index of refraction of 2.5. We expect to see a minimum in fractional reflection at $\lambda = 5/m$ millimeters, where $m = 1, 2, 3, ...$

We can make three other simple checks: as the index of refraction of a layer goes to ∞ we should see complete reflection (figure[2.5]); if both layers have the same index of refraction as air, we should see complete transmission (figure[2.6]); as $\theta \to \pi/2$ we should see complete reflection (figure[2.7]).

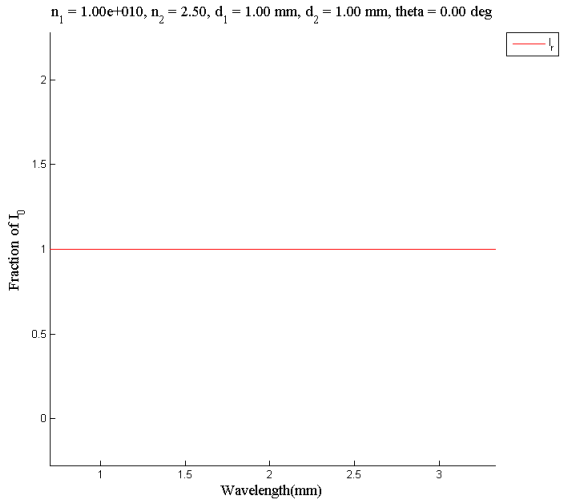

Figure 2.5: Two layer case where the first layer has index of refraction approaching ∞. We expect to see a total reflection.

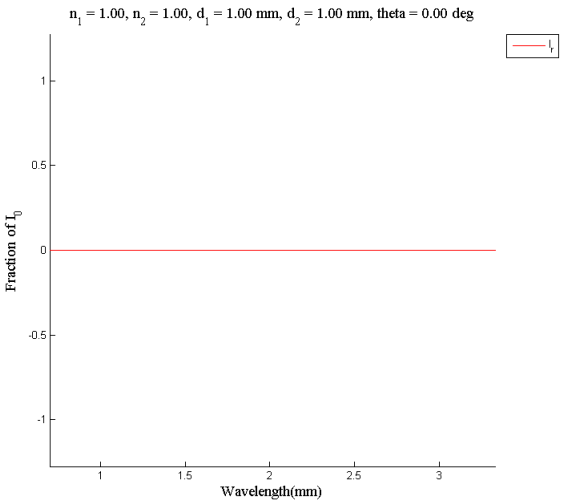

Figure 2.6: Two layer case where both layers are air. We see complete transmission, as expected.

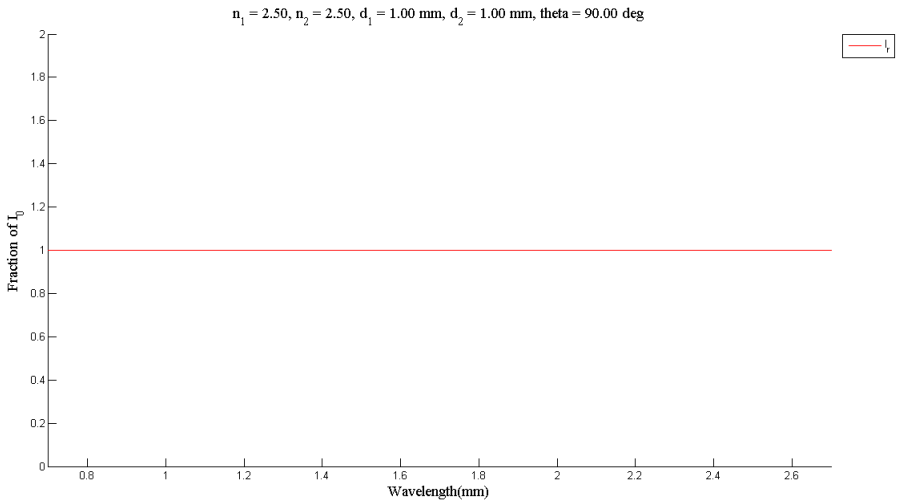

Figure 2.7: Two layer case where the angle of incidence is $\pi/2$. At this angle we expect to see total reflection.

Chapter 3

Three Layer Dielectric

3.1 Three Layer Case

We now add a third layer of dielectric material so our system looks like Air - Layer1 - Layer2 - Layer3 - Air.

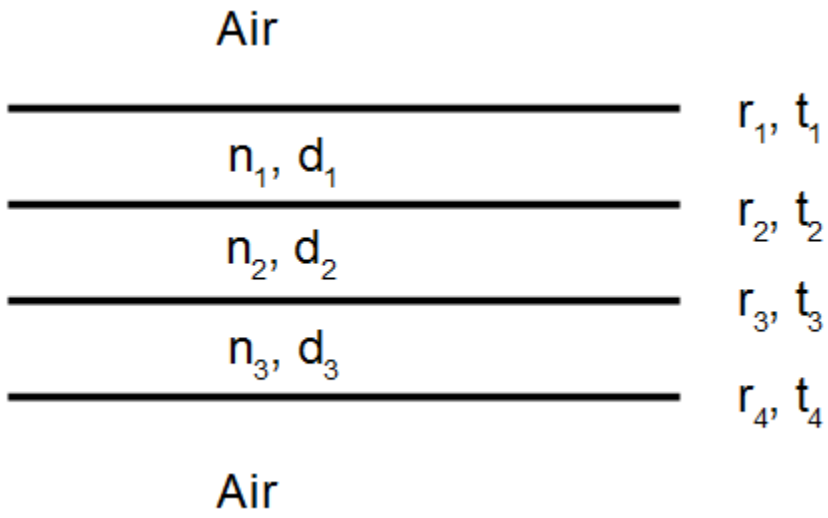

Figure 3.1: Schematic of Three Layer case

3.2 Calculating the Transmitted Field

We use the same process as before, and note that now any transmitted wave can be written as

$$E = t_1 t_2 t_3 t_4 (r_1 r_2 e^{-i\delta_1})^a (r_1 r_3 t_2^2 e^{-i(\delta_1+\delta_2)})^b (r_1 r_4 t_2^2 t_3^2 e^{-i(\delta_1+\delta_2+\delta_3)})^c$$
$$* (r_2 r_3 e^{-i\delta_2})^d (r_2 r_4 t_3^2 e^{-i(\delta_2+\delta_3)})^e (r_3 r_4 e^{-i\delta_3})^f$$

where $a, b, c, d, e,$ and $f = 0, 1, 2, ...$

This expression accounts for the reflections between any two layers occurring in any combination. To find the total transmitted field we sum all the possibilities. Using our infinite sum technique as previously, we conclude that

$$E_{tot} = \frac{t_1 t_2 t_3 t_4 e^{-i(3\delta_1+4\delta_2+3\delta_3)}}{(e^{-i\delta_1} - r_1 r_2)(e^{-i(\delta_1+\delta_2)} - r_1 r_3 t_2^2)(e^{-i(\delta_1+\delta_2+\delta_3)} - r_1 r_4 t_2^2 t_3^2)}$$
$$* \frac{1}{(e^{-i\delta_2} - r_2 r_3)(e^{-i(\delta_2+\delta_3)} - r_2 r_4 t_3^2)(e^{-i\delta_3} - r_3 r_4)}$$

3.3 Sanity Checks

First, we check that we see minima in fractional reflection where expected. If each layer has index of refraction equal to 2.5 and each layer is 1mm thick, we expect to see a minimum at $\lambda = 15/m$ millimeters (figure[3.2]).

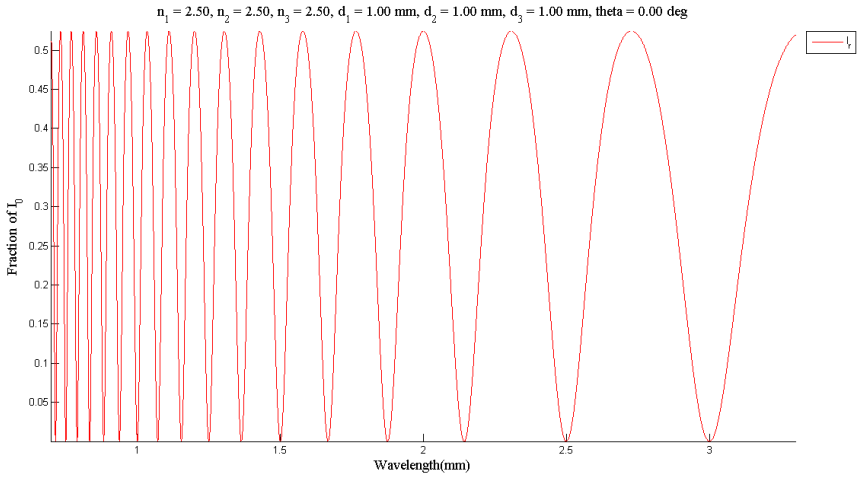

Figure 3.2: Three layer case where each layer has the same index of refraction. We expect to see a minimum in fractional reflection at $\lambda = 15/m$ millimeters

We can also check that the three layer case reduces to the two layer case by letting the first layer be air (figure[3.3]) and comparing to figure[2.3].

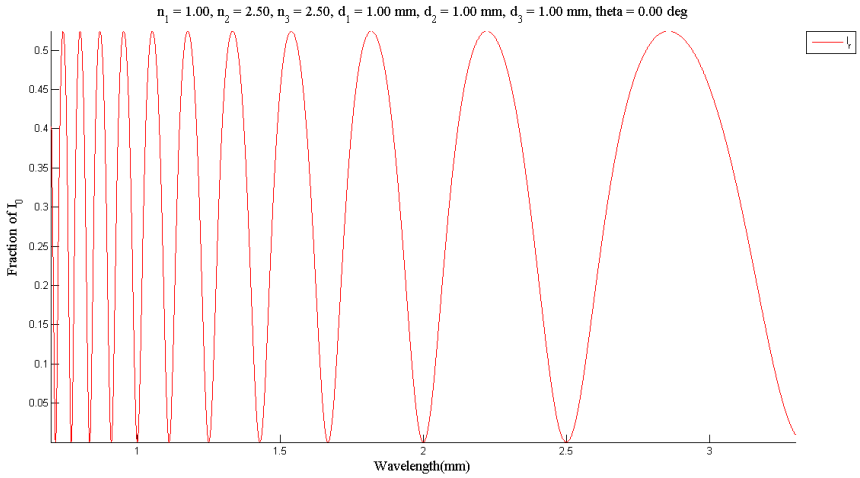

Figure 3.3: Three layer case where the first layer is air and the other two layers have the same index of refraction. We expect this case to be representative of the two layer case seen in Figure 2.3.

3.4 Quarter Stack

We can also observe the usefulness of our multilayer method by looking at quarter wavelength matching (figure[3.4]). The black line is drawn at a fractional reflection of 1%. Note the broad band minimum near 5mm that occurs by matching $n_1 = n_3 = \sqrt{n_2}$ and requiring $n_1 d_1 = \lambda/4$ [7]. We will see that by adding more layers we can improve the bandwidth of our minimum.

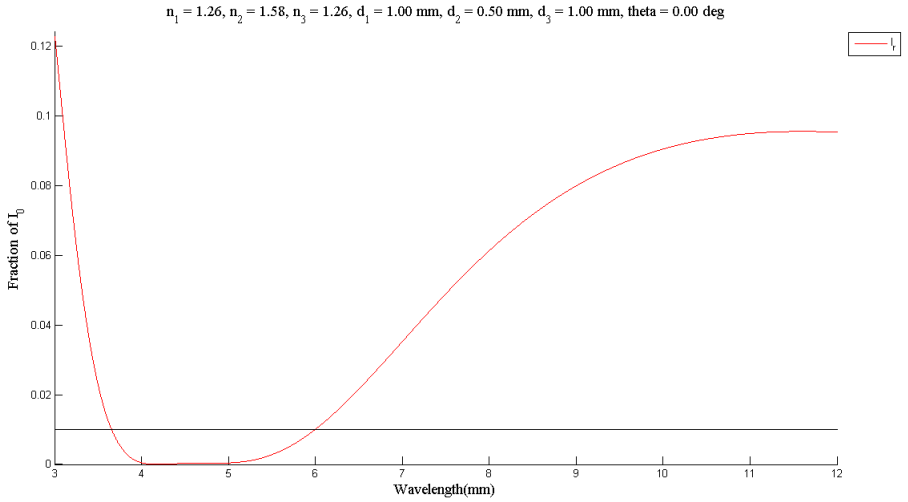

Figure 3.4: Three layer quarter stack case where $n_1 = n_3 = \sqrt{n_2}$. We expect to see a minimum at $\lambda = 4n_1 d_1 = 4 * 2.5^{.25} \approx 5.03$mm. This agrees with what the simulation shows.

Chapter 4

Five Layer Dielectric

4.1 Five Layer Case

We now add two more dielectric layers to our system which now looks like Air - Layer1 - Layer2 - Layer3 - Layer4 - Layer5 - Air.

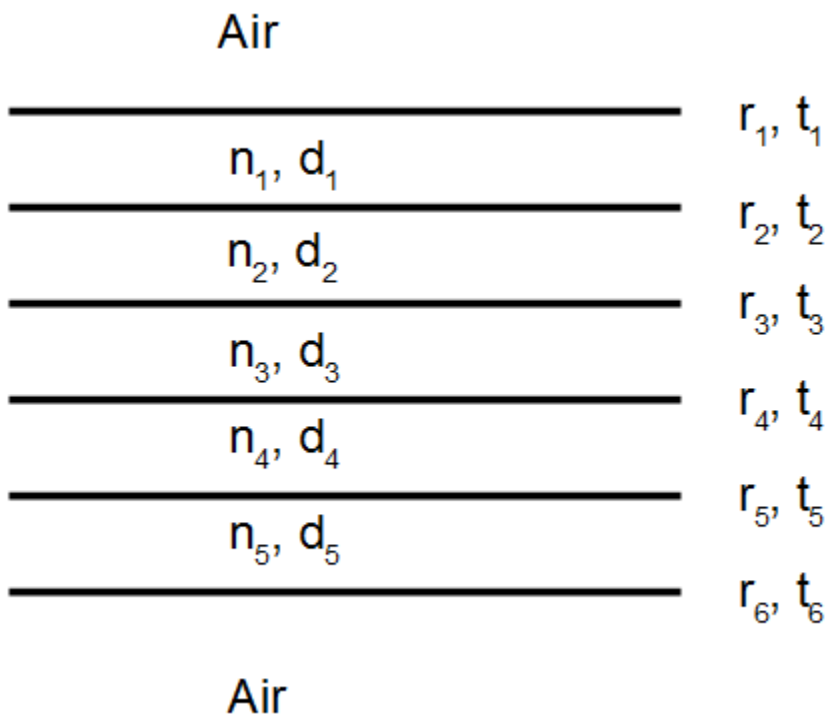

Figure 4.1: Schematic of Five Layer case

4.2 Calculating the Transmitted Field

Again, we can write any transmitted wave as

$$E = t_1t_2t_3t_4t_5t_6(r_1r_2e^{-i\delta_1})^a(r_1r_3t_2^2e^{-i(\delta_1+\delta_2)})^b(r_1r_4t_2^2t_3^2e^{-i(\delta_1+\delta_2+\delta_3)})^c(r_1r_5t_2^2t_3^2t_4^2e^{-i(\delta_1+\delta_2+\delta_3+\delta_4)})^d$$
$$* (r_1r_6t_2^2t_3^2t_4^2t_5^2e^{-i(\delta_1+\delta_2+\delta_3+\delta_4+\delta_5)})^e(r_2r_3e^{-i\delta_2})^f(r_2r_4t_3^2e^{-i(\delta_2+\delta_3)})^g(r_2r_5t_3^2t_4^2e^{-i(\delta_2+\delta_3+\delta_4)})^h$$
$$* (r_2r_6t_3^2t_4^2t_5^2e^{-i(\delta_2+\delta_3+\delta_4+\delta_5)})^i(r_3r_4e^{-i\delta_3})^j(r_3r_5t_4^2e^{-i(\delta_3+\delta_4)})^k(r_3r_6t_4^2t_5^2e^{-i(\delta_3+\delta_4+\delta_5)})^\ell$$
$$* (r_4r_5e^{-i\delta_4})^m(r_4r_6t_5^2e^{-i(\delta_4+\delta_5)})^n(r_5r_6e^{-i\delta_5})^o$$

This is a long expression, but actually very straightforward as we just need to look at all the possible reflections between any two layers. Computing this using nested for loops would have been tedious and long, as it would have required using 15 nested loops. Alternatively, we use the infinite sum method as before to find

$$E_{tot} = \frac{t_1t_2t_3t_4t_5t_6e^{-i(5\delta_1+8\delta_2+9\delta_3+8\delta_4+5\delta_5)}}{(e^{-i\delta_1}-r_1r_2)(e^{-i(\delta_1+\delta_2)}-r_1r_3t_2^2)(e^{-i(\delta_1+\delta_2+\delta_3)}-r_1r_4t_2^2t_3^2)(e^{-i(\delta_1+\delta_2+\delta_3+\delta_4)}-r_1r_5t_2^2t_3^2t_4^2)}$$
$$* \frac{1}{(e^{-i(\delta_1+\delta_2+\delta_3+\delta_4+\delta_5)}-r_1r_6t_2^2t_3^2t_4^2t_5^2)(e^{-i\delta_2}-r_2r_3)(e^{-i(\delta_2+\delta_3)}-r_2r_4t_3^2)(e^{-i(\delta_2+\delta_3+\delta_4)}-r_2r_5t_3^2t_4^2)}$$
$$* \frac{1}{(e^{-i(\delta_2+\delta_3+\delta_4+\delta_5)}-r_2r_6t_3^2t_4^2t_5^2)(e^{-i\delta_3}-r_3r_4)(e^{-i(\delta_3+\delta_4)}-r_3r_5t_4^2)(e^{-i(\delta_3+\delta_4+\delta_5)}-r_3r_6t_4^2t_5^2)}$$
$$* \frac{1}{(e^{-i\delta_4}-r_4r_5)(e^{-i(\delta_4+\delta_5)}-r_4r_6t_5^2)(e^{-i\delta_5}-r_5r_6)}$$

4.3 Sanity Checks

We again compute a couple limiting cases to ensure accuracy. Letting all the layers have index of refraction equal to 2.5 and thickness of 1mm, we expect to see minima in fractional reflectional at $\lambda = 25/m$ mm (figure[4.2]).

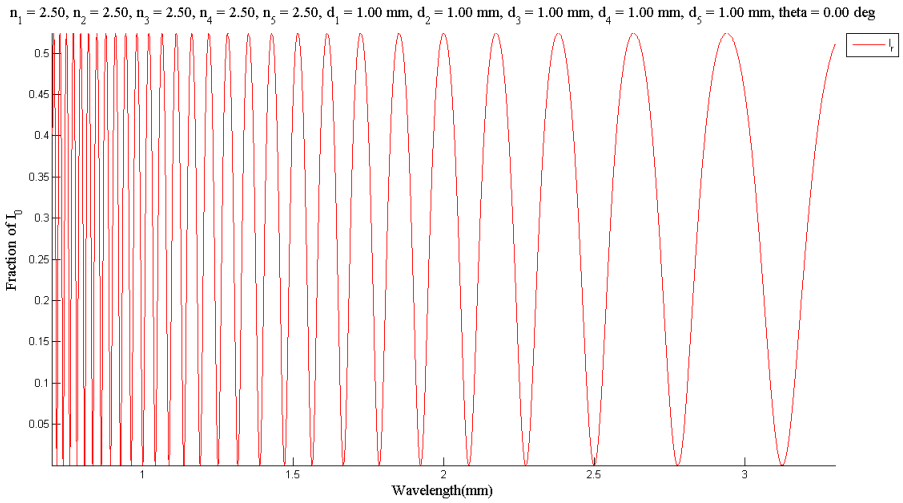

Figure 4.2: Five layer case where each layer has the same index of refraction. We expect to see a minimum in fractional reflection at $\lambda = 25/m$ millimeters.

We can also check that the five layer case reduces to the three layer case by letting the first two layers be air (figure[4.3]).

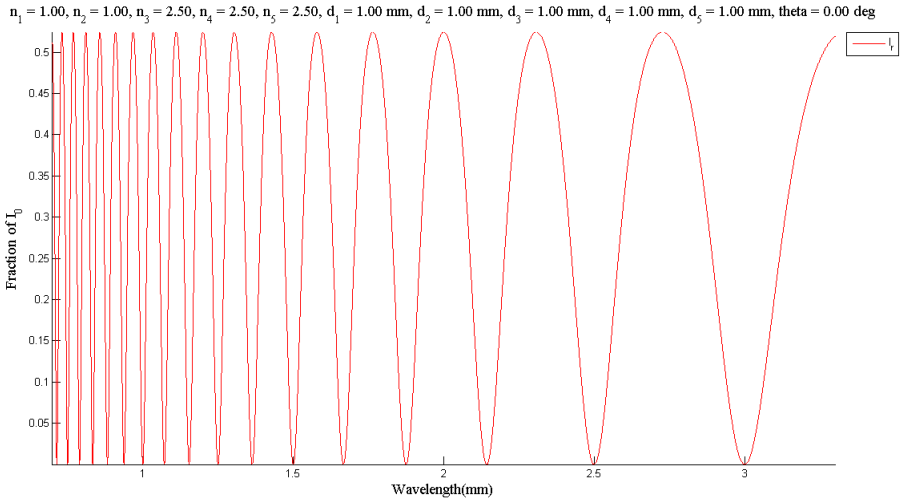

Figure 4.3: Five layer case where the first two layers are air and the remaining three layers have the same index of refraction. We expect this case to be representive of the three layer case seen in Figure[3.2].

4.4 Quarter-Quarter Stack

By simulating a quarter-quarter stack we can see the broadband effects for our multilayer AR coating. We let $n_1 = 2.5^{1/4}$ as in the quarter stack case, but now let $n_2 = 2$ and $n_3 = (n_2/n_1)^2$ [8] to produce a minima in fractional reflection. The black line is drawn at 1% fractional reflection. Note that for the quarter-quarter stack we see a fractional reflection of less than 1% from approximately 3.75 - 8mm (figure[4.4]). This is much better than the minima we see in the quarter stack case of approximately 3.75 - 6mm in figure[3.4].

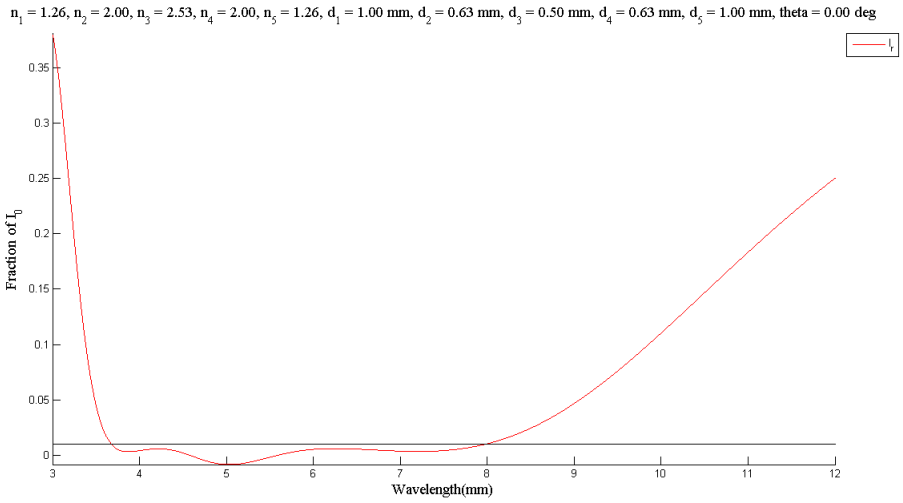

Figure 4.4: Five layer quarter-quarter stack case. We expect to see a minimum at $\lambda = 4n_1d_1 = 4 * 2.5^{.25} \approx 5.03$mm. This agrees with what the simulation shows. Note the broader minimum under 1% fractional reflection compared to that of Figure 3.4.

Chapter 5

Grooved Structure

Using thin films is not ideal for a very broadband AR coating. Alternatively, we suggest cutting parallel grooves into the lens material with a dicing saw (figure[5.1]). Cutting grooves that are much smaller than the wavelengths of the incoming light will allow the light to see an effective index of refraction that is less than the uniform material [6].

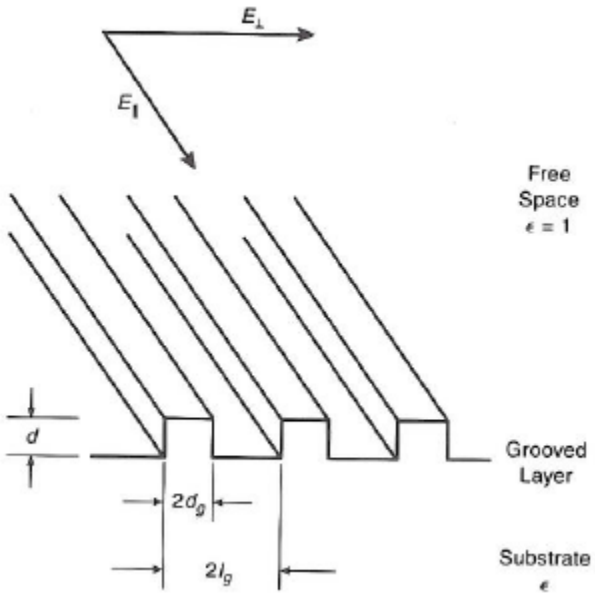

Figure 5.1: Schematic showing parallel grooves on a substrate of dielectric constant ϵ with grooves of width $2d_g$ and groove period of $2\ell_g$. This schematic reflects our two layer case where the first layer is the grooves and the second layer is a uniform dielectric. Note that there are two senses of polarization of light due to grooves being parallel [6].

We may additionally cut multiple layers of grooves at different depths and thicknesses, allowing us to choose whichever index of refraction we choose to create a quarter-quarter stack system that will allow for very broadband transmission. Because the structure is parallel grooves, the impedance will depend on the polarization the incoming light. We can treat the structure as a capacitor and find the capacitance per unit depth and length since $C = \epsilon \frac{A}{4\pi d}$, where A is the area of the plates, d is the distance between the plates (or groove thickness in our case), and ϵ will be the dielectric constant of the lens material. We can then simply find the impedance as $Z = 1/C$:

$$Z_{\parallel} = \frac{\ell_g}{d_g \epsilon + \ell_g - d_g}$$

$$Z_{\perp} = \frac{\ell_g - d_g}{\ell_g} + \frac{d_g}{\ell_g \epsilon}$$

From the impedance we can find the effective index of refraction for each sense of polarization. This method will allow for us to simulate what tolerances must be achieved in fabrication to result in a large bandwidth AR coating with satisfactory fractional reflection.

Chapter 6

Further Work

Further work includes using the model to simulate what tolerances must be achieved to result in a lens with a large bandwidth having less than 1% fractional reflection. We will integrate over beam, f/#, and wavelength. Loss also needs to be accounted for. Tolerances need to be known for the index of refraction of the silicon, groove depths, and groove thicknesses. Fabrication of the lenses will take place at NIST using a dicing saw to cut the grooves into the lenses. Testing using a Vector Network Analyzer will also be done at NIST to examine the reflection properties of the lenses after fabrication. We will also use a Fourier Transform Spectrometer at CU to test the lenses over a very large range of frequencies.

Chapter 7

Conclusions

We have shown the derivation, soundness, and usefulness of an analytic approach towards calculating the transmitted electric field through a multilayer dielectric system. The usefulness comes namely in the fact that we can achieve a broadband anti-reflection coating by using the quarter stack or quarter-quarter stack method. We note the improvement in bandwidth of minimum reflection of the quarter-quarter stack over the simpler quarter stack approach. This improvement can be seen below (repeat of figure[3.4] and figure[4.4]) in that the quarter stack approach shows fractional reflection less than 1% from approximately 3.75-6mm while the quarter-quarter stack shows fractional reflection less than 1% for approximately 3.75-8mm.

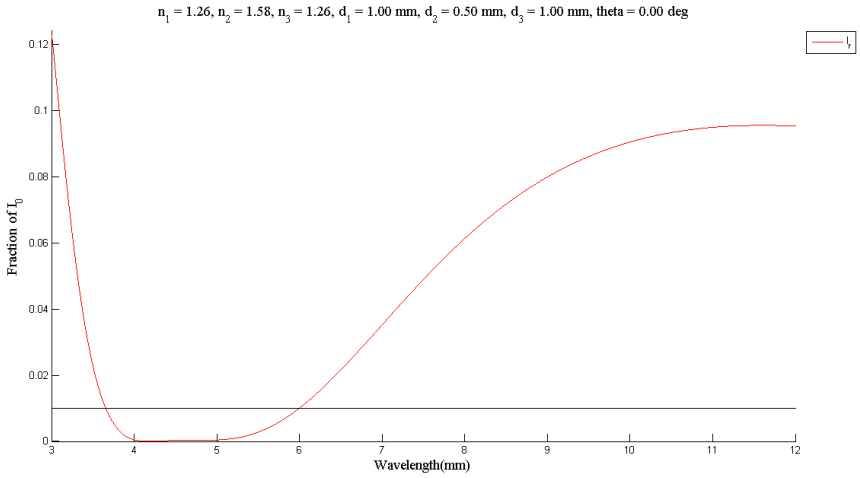

Figure 7.1: Three layer quarter stack case where $n_1 = n_3 = \sqrt{n_2}$. We expect to see a minimum at $\lambda = 4n_1d_1 = 4 * 2.5^{.25} \approx 5.03$mm. This agrees with the simulation.

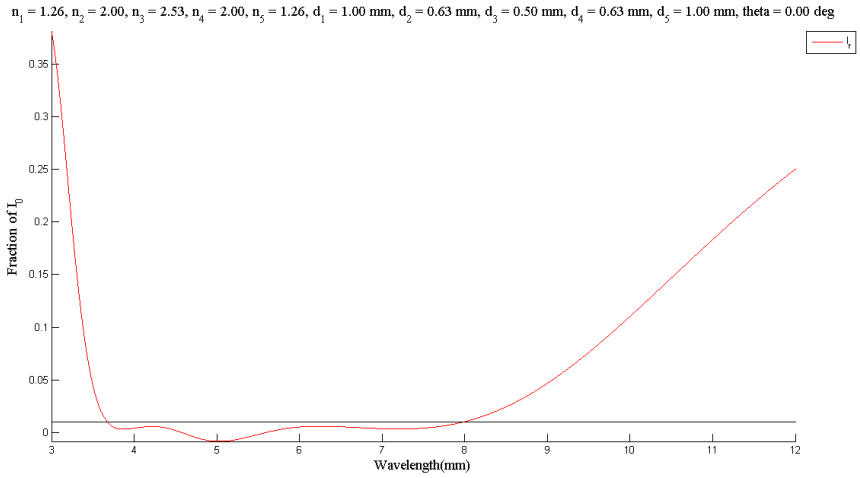

Figure 7.2: Five layer quarter-quarter stack case. We expect to see a minimum at $\lambda = 4n_1d_1 = 4 * 2.5^{\cdot 25} \approx 5.03$mm. This agrees with the simulation. Note the broader minimum under 1% fractional reflection compared to that of Figure 7.1.

We also note that to physically achieve the proper dielectric constants in fabrication that we can cut parallel grooves (figure[7.3]) into the silicon at different depths and widths as opposed to using thin films. By using the grooved method, we can control the effective dielectric constant that light sees given that the groove spacing is much less than the wavelength of the impeding light. This control will allow us to use index matching methods to create a broadband AR coating as demonstrated.

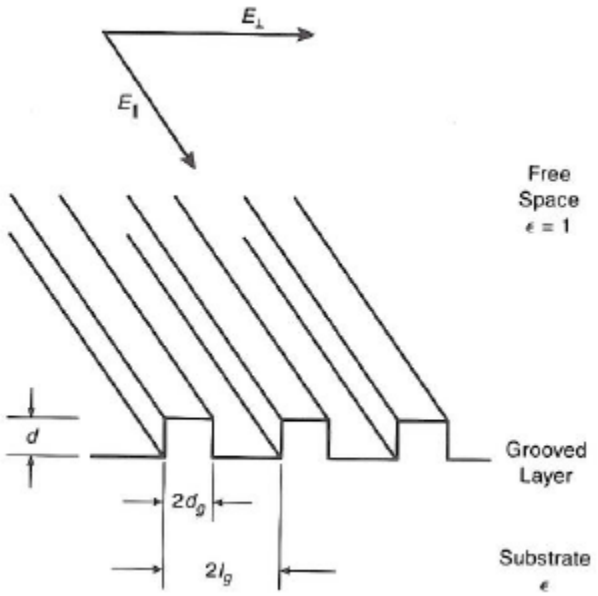

Figure 7.3: Schematic showing parallel grooves. Cutting the materical such that the groove spacing is much less than the wavelength of impeding light allows us to control the effective dielectric constant of the material. Ee can then use impedance matching techniques to achieve a broadband AR coating [6] .

Finally, we aim to use this model to simulate the tolerances that must be achieved during fabrication to result in fractional reflection of less than 1% across the desired bandwidth. We will be able to find the tolerances in material, groove thickness, and groove depth that must be realized to achieve the necessary AR coating. Testing after fabrication will take place at NIST and CU to verify our expectations.

Bibliography

[1] J. McMahon et al. Multi-Chroic Feed-Horn Coupled TES Polarimeters. astroph.IM/1201.4124 2012.

[2] CCAT website http://www.ccatobservatory.org/index.cfm 2012

[3] CCAT Design Team A Design Study for a Long-Wavelength Imager for CCAT (LWCam). 2012

[4] Gordon Stacey et al. SWCam: A Short Submillimeter Camera for CCAT. 2012

[5] Eugene Hecht Optics. Pearson 4th Edition 2002

[6] Paul F. Goldsmith Quasioptical Systems. IEEE Press 1998

[7] Max Born and Emil Wolf Principles of Optics. Cambridge Press 7th Edition 1999

[8] Jurgen R. Meyer-Arendt Introduction to Classical and Modern Optics. Prentice-Hall 2nd Edition 1984